



Dielectric properties, complex impedance analysis and electrical properties of novel particulate composites of NBT-SrFe₁₂O₁₉

Sunita Dagar¹ · Ashima Hooda¹ · Satish Khosa¹

Received: 28 March 2020 / Accepted: 31 May 2020 / Published online: 8 June 2020
© Springer Science+Business Media, LLC, part of Springer Nature 2020

Abstract

The proposed article describes the use of dielectric and complex impedance spectroscopy to evaluate various parameters such as electrical conductivity, activation energy, grain-grain boundary parameters, etc., of the $(1-x)\text{Na}_{0.5}\text{Bi}_{0.5}\text{TiO}_3-(x)\text{SrFe}_{12}\text{O}_{19}$; ($x=0.5, 0.8$ and 1) novel composite system formed with the help of solid-state reaction method. The composite samples have been achieved with modified and enhanced dielectric and electrical properties as compared to the pure ferroelectric and hexaferrite phase before making their composites. Both the regions of low dielectric constant and higher dielectric constant reveal the presence of Maxwell–Wagner polarization. The distribution relaxation time, Cole–Cole plot, and comparison of Modulus and impedance plot disclose the presence of space charge polarization and constant phase element justifying the semiconductor behavior of the samples. The overlapped normalized impedance curve on a single master curve confirmed the presence of relaxation phenomena in the samples and revealed that the samples follow a single relaxation phenomenon at all the temperatures. Jonscher’s power law has been used to find different models of conduction.

1 Introduction

Biphasic particulate composites with simultaneous coexistence of ferrite and ferroelectric phases are mainly exploited as magnetic sensors [1]. Their coupled magnetic and ferroelectric properties are expected to develop a small size and smarter electronic components [2–4]. However, the hexaferrite is also promising for practical use as single-phase magnetoelectric material. This is the class of hexaferrite, which combine in single-phase a good ferromagnetic and ferroelectric properties [5–7]. Furthermore, large spontaneous polarization and multiferroic properties at room temperature recently discovered in barium hexaferrite substituted by diamagnetic cations [7]. Herewith the magnetoelectric characteristics of M-type hexaferrite fabricated by a modified ceramic technique are more advanced than those for the well-known room temperature BiFeO₃ orthoferrite multiferroic [8, 9]. Moreover, to make laminate and particulate composites of ferromagnetic and ferroelectric materials is well approach. The doped ferrites and titanates are suitable

candidates for composite multiferroics [10, 11]. When the biphasic ME composites are subjected to the magnetic field then electric polarization is generated [12, 13] which is based on several factors but amongst them, conduction phenomena in component phases are of prime importance [7, 14]. Also, the ME output has been investigated in terms of dc conductivity [1]. However, still, no detailed studies are available on the role of dielectric and electrical phenomena towards magnetic and electric interactions for the case of composite systems. The resultant electrical phenomena in polycrystalline materials are greatly influenced by grain, grain boundary, and solid-electrode interface, as these all contribute to the total conductivity [7, 14]. To reduce the polarization effects and to gain deeper information about electrical conduction and different mechanisms involved in it ac technique can be very fruitful. Investigations of complex impedance and their equivalent circuit modeling lead towards the real value of bulk conductivity. Also, the frequency-dependent behavior of conductivity is helpful to find out various models associated with the conduction phenomena. The hopping phenomena of mobile charge carriers can be explained and offer a unique opportunity to study the movement of a charged particle on a variety of time scales and is rightly called a powerful microscope from time to time [7]. Various dielectric relaxations can be investigated and the shift of dielectric transition temperature would lead

✉ Ashima Hooda
ashima1686@gmail.com

¹ Material Research Laboratory, Department of Physics, Deenbandhu Chhotu Ram University of Science and Technology, Sonapat, Haryana 131039, India

towards the signature of the ME effect present in the specimen [7, 14].

As it is clear from the aforementioned literature and our previous studies [7, 14] that the dielectric measurements give fruitful information about the ME coupling [7] and composites of ferrites with NBT provide fruitful results. Hence we are inspired to communicate the complex impedance analysis and fascinating dielectric behavior of novel composites of $\text{Na}_{0.5}\text{Bi}_{0.5}\text{TiO}_3$ (NBT)- $\text{SrFe}_{12}\text{O}_{19}$ (SM) as a function of frequency as well as temperature.

2 Experimental

Although Almessiere et al. [15]. have developed nanocomposites using citrate sol–gel method. However, the solid-state reaction method has various advantages such as simple to perform, lower cost, ecofriendly, better filling properties, and the final product is structurally authentic accompanying fascinating properties. Hence we adopted solid-state reaction method [16] to synthesized the novel ceramic composites with general formula $(1-x)\text{Na}_{0.5}\text{Bi}_{0.5}\text{TiO}_3-(x)\text{SrFe}_{12}\text{O}_{19}$; ($x=0.5, 0.8$ and 1). In this method, all the initial constituents were weighed and mixed in a stoichiometric amount [7, 16]. The mixture was grounded to get a homogeneous mixture and then calcinated at $800\text{ }^\circ\text{C}$ for 4 h and then finally sintered at $1100\text{ }^\circ\text{C}$ for 4 h. The phase formation was confirmed using XRD miniflex-II and a small Fe_2O_3 peak is observed only in $x=0.5$ (higher ferroelectric component), which does not affect properties. To have dielectric measurements pellets of the sintered samples have been formed with a die set of 10 mm with a thickness of nearly 1–1.5 mm and then silver polling is done, to make strong electrodes heat treatment is done at $120\text{ }^\circ\text{C}$ overnight. Hioki 3532-50 LCR Hi-Tester set up was used for dielectric and impedance studies from RT to $480\text{ }^\circ\text{C}$. To study electrical (dc) phenomena Keithley 2401 source meter is used from RT to $400\text{ }^\circ\text{C}$ at the rate of $2^\circ/\text{min}$. All the dielectric and electrical parameters are

calculated using the formulas as discussed in our previous reports [7, 14].

3 Results and discussions

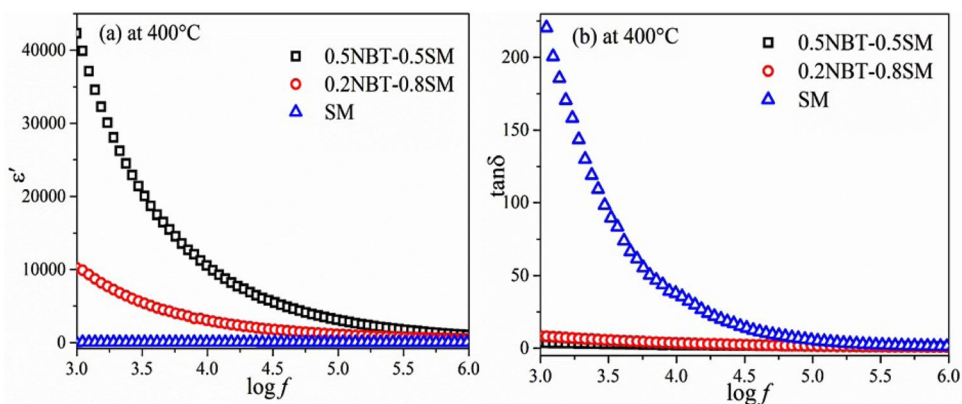
3.1 Impedance spectroscopy (IS)

Impedance spectroscopy is a powerful tool for investigation of electrical properties of a system i.e., polycrystalline system, inhomogeneous structures, and electrode interfaces, etc. It is significant to describe the dynamic behavior of static and mobile charges [17].

3.1.1 Dielectric investigations

The compositional variation of dielectric constant and loss as a function of frequency is put on display in Fig. 1. The observed behavior exhibits higher values of both the parameters and then starts decreasing as the frequency is move to higher values, this decrease becomes slow after a certain high frequency (i.e., approaching towards constant values). A rapid decrease in ϵ' values is observed at lower frequencies than at higher frequencies because materials under applied external electric field exhibit induced dipole moment [18]. Higher dielectric constant at smaller frequencies is not only intrinsically, but the heterogeneous conduction in the biphasic composites is also responsible for it [19] which arises on account of interfacial polarization as per Maxwell–Wagner model [20] and well agreed with the phenomenological theory of Koop's model [18, 21]. All types of polarizations like electronic, ionic, orientational, and space charge (most important) contribute to the dielectric constant at lower frequencies [22]. In smaller frequency regions, extra mobile charges start collected near grain-grain boundaries interfaces enlarging polarization, resulting in larger dielectric constant. On the contrary, with the increase of frequency, more and more polarization could not synchronize with the frequency hence dielectric constant decreases [23]. As the

Fig. 1 Frequency variation of **a** dielectric constant (ϵ') for all the synthesized compositions at $400\text{ }^\circ\text{C}$ and **b** tangent loss ($\tan\delta$) at $400\text{ }^\circ\text{C}$



ferroelectric particles are surrounded by ferromagnetic regions, account for such behavior in composites as that of relaxors [13, 24]. The loss tangent follows a similar pattern as dielectric constant and is in accordance with Koop's double layer model. According to the model, the charge carriers require more energy to move at smaller frequencies, and hence $\tan\delta$ is large. However, smaller energy is sufficient to surpass the energy limits and leads to reduced $\tan\delta$ values [18]. Although, composites acquire higher dielectric constant values, dielectric constant decreases in incorporating SM hexaferrite in the NBT phase which might be possibly due to dilution of ferroelectric polarization or lower dielectric constant of hexaferrite phase [24, 25]. The appearance of additional cationic or electron vacancies due to charge imbalance, there might be a decrease of strontium concentration which can decrease the dielectric constant [26]. As in ferrites, there are both kinds of charge carriers i.e., electrons and holes, and holes mobility is relatively lower than electrons and in the opposite direction. As the ferrite content increases both n-type and p-type carriers increase and the contribution of holes towards polarization decreases even at lower frequencies hence may lead towards lower dielectric constant [27].

Figure 2a depicts the compositional variation of dielectric constant (inset $\tan\delta$) at 35 kHz and b for pure SM hexaferrite at different frequencies as a function of temperature. It is noticed that both dielectric constant and $\tan\delta$ increase whole with temperature up to a maximum value and thereafter begin to decrease. For smaller temperatures dipoles could not catch up with the applied electric field, thereby lowering polarization, and hence dielectric constant decreases. However, in high-temperature regions, they are brought about with sufficient heat energy to align themselves in field direction and give rise to a resultant higher polarization which is the basic condition for dielectric constant to be increased. Transition temperature decreases on increasing SM hexaferrite content because of the presence of both kinds of charge carriers i.e., n-type (electrons) and p-type (holes) [7]. The

relative mobility of p-type carriers is smaller than n-types and in the opposite direction, and plays a significant role in polarization mechanism at higher temperatures causing the observed decrease of dielectric constant [7, 27]. In pure hexaferrite, a continuous rise of dielectric constant is noteworthy the transition temperature which is probably due to electron/hole displacement in the ferrite phase [7, 14]. As the, thermally activated charge carriers increased with temperature, their mobility increase resulting in higher conductivity and all of these factors increase the tangent loss. There is a shift of transition temperature disclosing the presence of the ME effect in these samples [7, 12, 14]. Dielectric behavior near the transition region can be interpreted on the behalf of domain wall motion. The domain walls are unable to move at lower temperatures and contribute less to the dielectric constant, but become dominant at transition temperatures and exceed the dielectric constant. Moreover, above the transition temperature dielectric constant reduced because it is very difficult to adjust the accelerated random vibrational motion with the applied field [7, 14]. Furthermore, composite samples having minimum losses and larger dielectric constants are obtained, which could be potential candidates for various applications.

3.1.2 Complex impedance analysis

Simulated complex impedance curves of the developed system at 400 °C and for $x=0.5$ at various temperatures are illustrated in Fig. 3. These curves are of semielliptical shape rather than a perfect semicircle disclosing the Non-Debye kind relaxations. After the simulation, these curves are found to have two overlapping semicircles having their centers slightly below the real z-axis, hence follow Maxwell double layer model. The high frequency smaller circle with smaller relaxation time formed due to conductive grains is merged in lower frequency circle with larger relaxation time corresponding to grain boundary [28]. A decrease in the diameter of the depressed semicircular is noticed when the

Fig. 2 a, b Temperature variation of dielectric constant (ϵ') and (inset) tangent loss ($\tan\delta$) for all composites at 35 kHz frequency and for SM at different frequencies, respectively

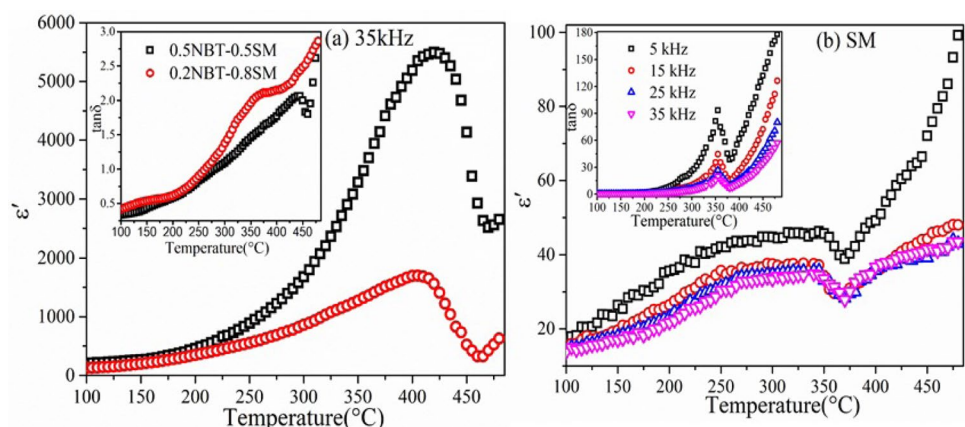
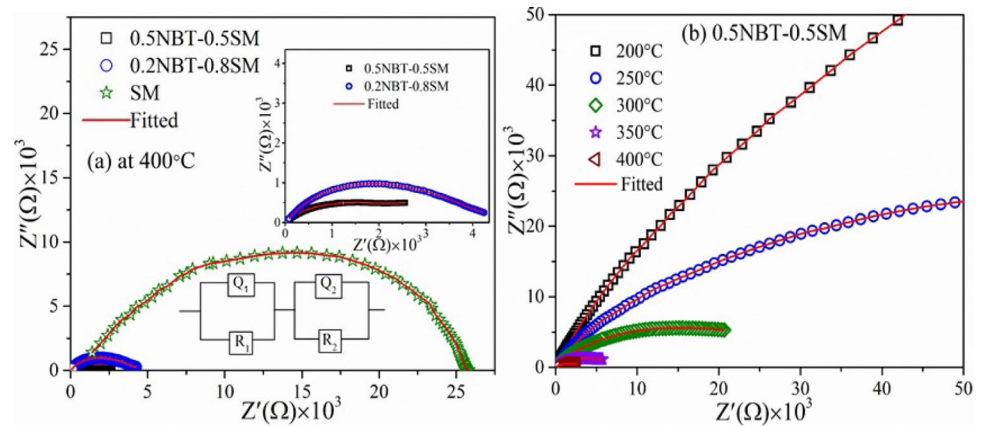


Fig. 3 **a** Fitted Nyquist plot of impedance for all compositions at 400 °C along with equivalent circuit **b** for 0.5NBT-0.5SM at different temperatures



temperature rises revealing the decrease in real resistance which exhibits the typical semiconducting behavior of the samples.

The modeled equivalent circuit (Fig. 3a) for the samples consists of serially connected parallel combination of two R-CPE(constant phase element) elements. The constant phase elements are put in place of the ideal capacitor to justify the Non-Debye type behavior appears because of distribution of relaxation time, the roughness of sample surface, etc. of the impedance plots. The complex impedance curves are fitted using EC.lab software as discussed in previous studies [7, 14]. Various fitted parameters grain, grain boundary resistances (R_1 and R_2), grain and grain boundary capacitances (C_1 and C_2), constant phase elements (Q_1 and Q_2), and relaxation time distributions (α_1 and α_2) are tabulated in Table 1 for $x=0.5$ composition at different temperatures. Here values of α vary between ~ 0.5 and ~ 0.7 representing non-Debye type of relaxation behavior [7, 14]. Other compositions behave analogously.

As the plot of the imaginary part of complex impedance (Z'') as a function of frequency at logarithmic scale for samples at different temperatures is shown in Fig. 4. These plots exhibit a decline of Z'' with increasing temperature indicating towards increase in conductivity which is related to electron hopping phenomena. Hence, it is clear that electron hopping is a thermally activated process that increased with temperature and is the reason for higher conductivity at higher temperatures. The observed peaks in these

plots correspond to the relaxation phenomena and appear at a relaxation frequency (f_m). As the relaxation frequency is taken as the reciprocal of the minimum time taken by the electrons to reorient them in the applied field direction which is responsible for the frequency-dependent behavior of dielectric constant. When the dielectric material is subjected to electric field it gets polarized due to induced dipoles. With each direction reversal, the dipoles try to reorient themselves in the field direction, but the process takes some finite time called the relaxation time. Also, a dipole could not keep shifting orientation direction when the frequency of the applied exceeds its relaxation frequency and no contribution to the dielectric constant. So, the observed shift of these broad peaks towards larger frequencies with the rise of temperature is due to this relaxation time at which the electrons are unable to follow the frequency of applied field greater than their relaxation frequency and results in a decreased dielectric constant at higher frequencies [22]. Also, it is noteworthy that as the ferrite phase is increasing the shift of peaks towards the higher frequency side is also increasing revealing the increased electron hopping process. Hence, it is concluded that all the consequences obtained, dependent on electron hopping are due to the ferrite phase.

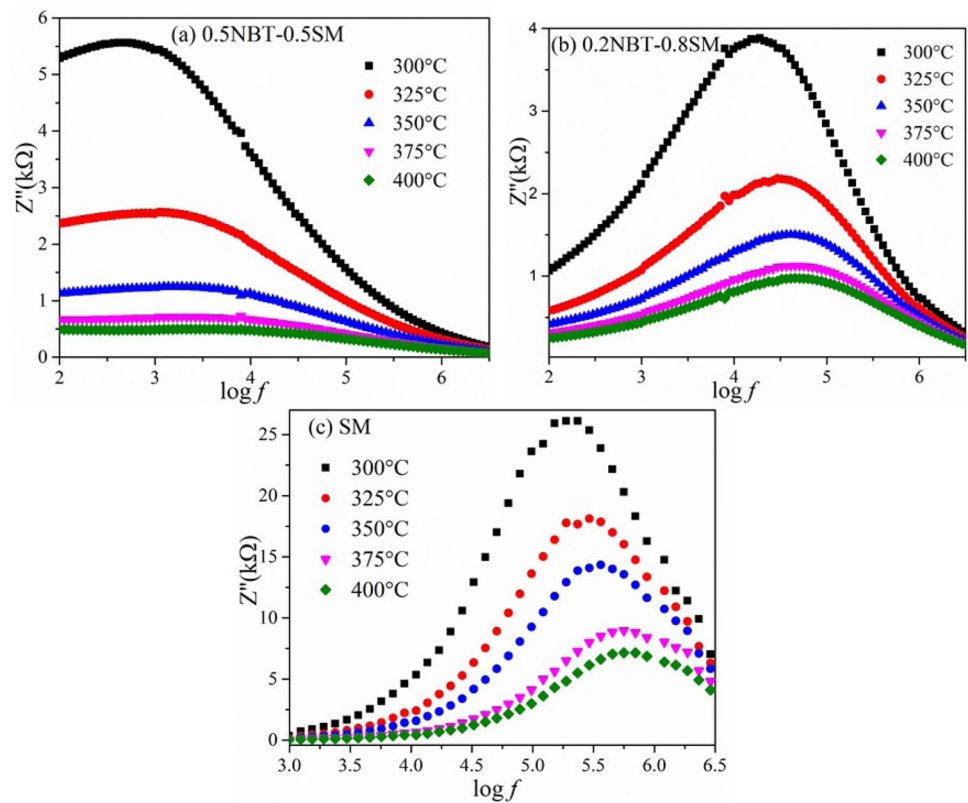
3.1.3 Scaling behavior of impedance

To check whether the relaxation phenomena are exactly occurring or not occurring in the specimen a normalized

Table 1 Grain, grain boundary parameters of 0.5NBT-0.5SM obtained from the fitting

T (°C)	R_1 (K Ω)	R_2 (K Ω)	C_1 (nF)	C_2 (nF)	Q_1 (CPE $_1$) (nFs $^{(\alpha_1-1)}$)	Q_2 (CPE $_2$) (nFs $^{(\alpha_2-2)}$)	α_1	α_2
200	96.27	558.86	1.04	5.07	16.16	31.59	0.71	0.68
250	16.93	87.30	1.53	10.17	45.92	151.20	0.70	0.62
300	4.92	22.55	2.63	18.29	153.20	582.10	0.63	0.57
350	2.45	4.88	3.64	82.52	491.00	3756.00	0.57	0.51
400	1.49	2.14	5.65	549	1516.00	22,550.00	0.45	0.52

Fig. 4 Variation of imaginary part of impedance (Z'') with logarithm of frequency ($\log f$) for prepared samples at different temperatures



complex impedance (Z''/Z''_{\max}) is plotted with normalized frequency (f/f_m) at logarithmic scale for different temperatures (Fig. 5). The f_m is the maximum frequency corresponding to Z''_{\max} . The overlapped normalized impedance curve on a single master curve confirms the presence of relaxation phenomena in the samples and shows that the samples follow a single relaxation phenomenon at all the temperatures.

To check the presence of space charge polarization effect and constant phase element a plot representing the comparison of imaginary complex impedance and electric modulus versus frequency is shown in Fig. 6. It is found that Z'' shows relaxation peak at lower frequencies and M'' at higher frequencies hence. They behave differently in symmetry and peak positions revealing the presence of space charge polarization and proposes the non-Debye behavior and rationalizes the presence of constant phase element in the fitting of the circuit [29]. No overlapping temperature could be observed in the entire temperature range, exhibiting both long-term conductivity and localized components for relaxation in the developed ceramics [29, 30]. If the peaks in the combined plots of Z'' and M'' versus frequency appear at the same frequency, then the charge carriers possessing long-range mobility are involved in the relaxation mechanism [31].

3.2 Electrical characterizations

3.2.1 Dc conductivity

The variation of dc conductivity of developed specimens as a function of the inverse of temperature is shown in Fig. 7a and the conductivity isotherm is linearly fitted to get the activation energy using the formula as given in our previous studies [7, 14]. The values of both dc conductivity and activation energy are given in Table 2. Various factors are affecting the ionic dc conduction such as number of charge carriers, temperature, defects, or distortion in structure and activation energy required for successful hop of ions from one site to another vacant site. Jumping ions with higher charge experienced a larger energy barrier to jump over various neighboring vacant sites [32, 33]. The dc conductivity of hybrid composite samples is higher than that of strontium hexaferrite and NBT [14] and kind of behavior might be attributed to an excess of charge carriers or oxygen vacancies created during synthesis. Generally, oxygen vacancies, Bi deficiency, and dipolar defects, etc. are attributed to the dc conductivity behavior in ferroelectrics [29, 34]. In our previous studies, it has been found that the biphasic composites experience octahedral distortions [7, 14]. Usually, these distortions might be due to defect vacancy mechanism i.e.,

Fig. 5 The scaling behavior of Z'' (imaginary part of impedance) of prepared composites

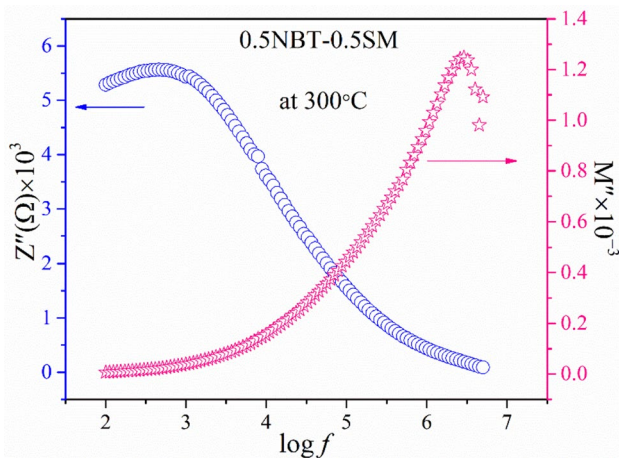
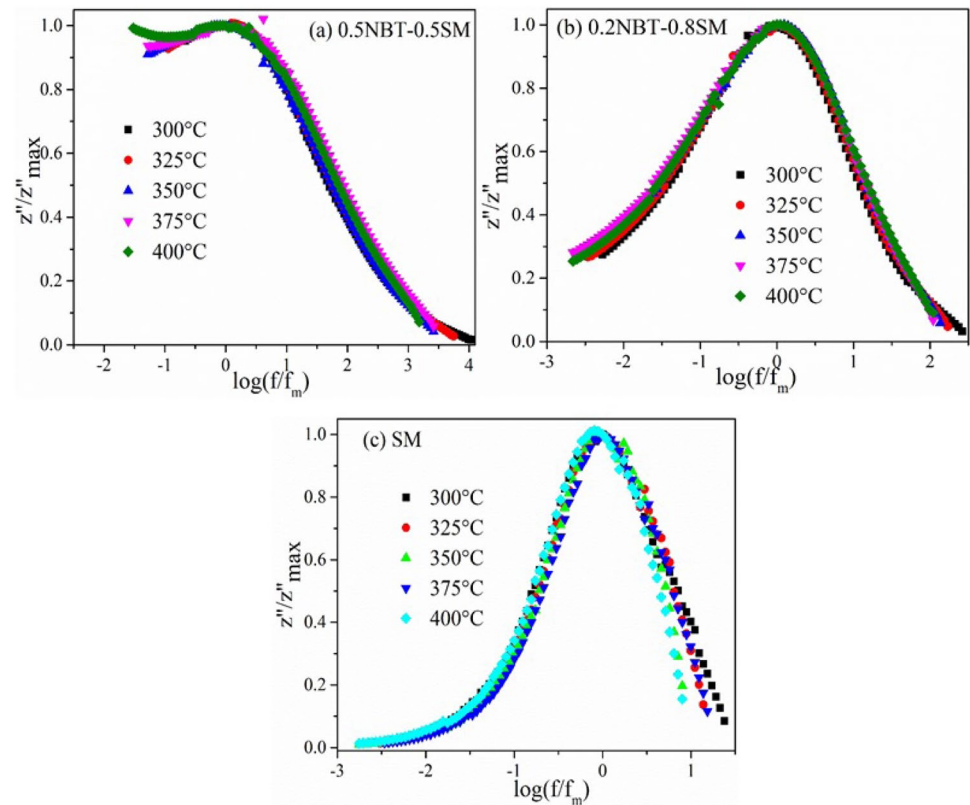


Fig. 6 Frequency versus imaginary electric modulus (M'') and imaginary impedance (Z'') at 300 °C for $x=0.5$

cationic or oxygen vacancies. Oxygen excess and deficit can increase and decrease the oxidation degree of 3d-metals. The changing of the charge state of 3d-metals as a consequence of changing of oxygen content changes such magnetic parameters as total magnetic moment and Curie point and such electrical parameters as resistivity and bandgap [35, 36]. Moreover, oxygen vacancies effect on exchange interactions. The intensity of exchange interactions decreases with

oxygen vacancy concentration increase leading towards higher conductivity [37, 38]. It is supposed that in composites $Ti(d^0)$ gives its electron to $Fe(3d^6)$ and creates an oxygen vacancy to compensate charge imbalance. However, dc conductivity in hexaferrite is usually characterized by Verwey hopping mechanism [39]. But in ferrites, 3d-Fe and 2p-O band gap is expected to be decreased with an increase in the oxygen vacancy concentration which would lead to a rise in electrical resistivity in them and increase the oxide ion conductivity [35]. Also, these vacancies increase with temperature reasonably increase the oxide ion conductivity rather than electronic conduction.

The mass transport of oxygen vacancies can be understood by the concept of space charge situation observed in various ionic as well as mixed ionic-electronic conductors. Usually, both ferrite and ferroelectric ceramics are supposed to have grain and grain boundaries, and also in biphasic materials, there is an interface between the two phases that can be considered. So, basically due to higher diffusion gradient oxygen vacancies at positively charged grain boundaries [40] than bulk creates space charge regions as a blocking layer for oxygen vacancy conduction. The oxygen-poor micro-domains appear on the grain surface. As a result, the electron transfer between grains is difficult and the conductivity decreases. Hence the increased concentration of oxygen vacancies will leads to broadening in this depletion width thereby decreasing the electrical conductivity [26, 35,

Fig. 7 **a** Arrhenius plot of dc conductivity (σ_{dc}) for all prepared samples, **b** frequency dependence of ac conductivity for all samples at 400 °C, **c** Frequency variation of ac conductivity (σ_{ac}) for 0.5NBT-0.5SM at different temperatures and **d** temperature variation of s parameter

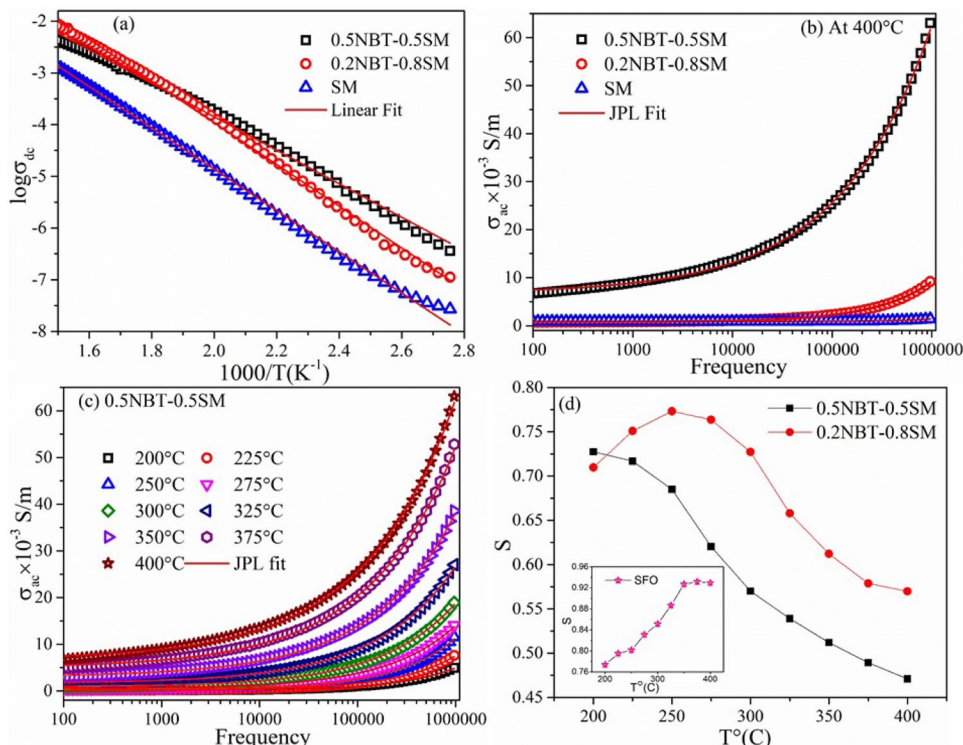


Table 2 The dc conductivity (σ_{dc}), activation energy (E_{dc}), of all the synthesized ceramic samples

Sample	σ_{dc} (10^{-3} S/m) at 400 °C	E_{dc} (eV)
0.5NBT-0.5SM	4.54	0.64
0.2NBT-0.8SM	8.81	0.80
SM	1.50	0.79

41]. This space charge polarization is related to the dielectric constant and hence conductivity varies with temperature analogously as dielectric constant varies with temperature. However, for the mesoscopic system when the Debye lengths become comparable with the grain size then a large change in conductivity can be noticed.

3.2.2 Ac conductivity

JPL fitted ac conductivity curve of all the compositions is put on display in Fig. 7b. Having their variation with frequency on the logarithmic scale. It is noteworthy, that ac conductivity shows a straight region when the frequency is minimum and then rises with the frequency. The lower frequency behavior of ac conductivity is the result of the polarization effect at the electrode–electrolyte interface. This can be explained by the Maxwell–Wagner model and Jump relaxation model (as discussed in our previous study [7]. When the applied frequencies are smaller than all the

charges accumulated at the conducting grain and insulated grain boundaries and hence reduces the charge carriers in the interior of the specimen, due to which the hopping of electrons between the ferric/ferrous ions of the ferrite phase reduces and hence leads to constant values at these frequency values. But conductivity varies linearly with frequency which is probably on account of hopping of electrons between two pairs of localized states [7]. When the applied frequencies are higher enough then the outer electrons in the dielectric material detached from the atom and the dielectric material becomes a conductor hence conductivity increased. Also from the fitted Cole–Cole plot of impedance it is clear that at lower frequencies grain boundaries are active; however, at higher resistance higher frequency conduction is due to active grains of lower resistance. Hence there is a prominent effect of grain and grain boundaries on conductivity.

Again, the temperature effect on ac conductivity is analyzed for 0.5NBT-0.5SM at different temperatures and put on display in Fig. 7c. The ac conduction increases with temperature due to the increased mobility of thermally activated charge carriers. All samples behave similarly. Also, the conduction phenomena dependent on the bond distances between the Fe^{2+} and Fe^{3+} ions at octahedral sites, as the distance decreases then electron hopping increases between them, and conductivity increases. With the incorporation of the SM phase in the ferroelectric NBT matrix, conductivity increases because of increased charge carriers and decreasing bond distances between ferric ions at octahedral sites.

Also, the created oxygen vacancies in perovskites either intrinsically or extrinsically (as reported in previous papers) would lead to higher conductivity [7, 14].

3.2.3 Conductivity models

Various models are suggested for the conductivity mechanism on account of the behavior of frequency exponent ' s ' towards frequency and temperature. The s parameter is calculated by fitting the ac conductivity curve with Jonscher's power law as discussed in previous studies [7, 14] and its temperature dependency is put on display in Fig. 7d. If the values of s are less than 1 then there is a translation hopping and if greater than 1 then the hopping will be localized [4]. In the present case, all the samples have s values less than 1 hence corresponds to translational hopping. Generally, these models include [14] (i) quantum mechanical tunneling model (QMT) which is valid only when the s is temperature independent, (ii) correlated barrier hopping (CBH) and appears if s parameter decreases with temperature and (iii) Overlapping large polaron tunneling model (OLPT) is suggested when s found to decrease with temperature up to a minimum value and then again increases with further increase in temperature. In this model, the Coulomb potentials at the two sites overlap, thus producing large overlapping polaron clouds, thereby reducing the polaron hopping energy. Hence from Fig. 7d, it is found that a small polaron tunneling model (NSPT) is associated with pure strontium hexaferrite, inverse OLPT model is associated with $x=0.5$ and $x=0.8$ follow CBH model of conductivity.

4 Conclusions

The fruitful solid solutions of NBT with SrFe₁₂O₁₉ Hexaferrite with formula $(1-x)\text{Na}_{0.5}\text{Bi}_{0.5}\text{TiO}_3-(x)\text{SrFe}_{12}\text{O}_{19}$; ($x=0.5, 0.8$ and 1) has been developed successfully. The dielectric constant is found to increase with the ferroelectric phase and enhanced as compared to both the constituent phases. Very large values of dielectric constant make them suitable for high-temperature ceramic capacitors. Enhanced dielectric constant and shift of impedance peak towards higher frequency side with increasing temperature discloses the presence of thermally activated electron hopping. The calculated resistance and capacitance values of grain boundaries are higher than grains. The overlapped normalized impedance curve on a single master curve confirms the presence of relaxation phenomena in the samples and shows that a sample follows a single relaxation phenomenon at all the temperatures. The increase of dc conductivity with temperature and composition is expected to be due to oxygen vacancies. Non-overlapping small polaron tunneling model (NSPT) is associated with pure strontium hexaferrite, inverse

OLPT model is associated with $x=0.5$ and $x=0.8$ follows CBH model of conductivity. Ac conductivity decreases with the addition of hexaferrite and increases with temperature and frequency well agreement with Jonscher's power law.

Acknowledgements Sunita Dagar would like to thank the Project Implementation Unit (NPIU), a unit of Ministry of Human Resource Development, Government of India, for the financial assistantship through TEQIP-III Project at Deenbandhu Chhotu Ram University of Science and Technology, Murthal, Haryana.

Compliance with ethical standards

Conflict of interest The authors declare no conflicts of interest.

References

1. K.K. Patankar, S.A. Kanade, D.S. Padalkar, B.K. Chougule, *Phys. Lett. A* **361**, 472 (2007)
2. R. Pattanayak, S. Panigrahi, *J. Magn. Magn. Mater.* **481**, 162 (2019)
3. V. Singh, K.K. Singh, Bamzai. *Mater. Chem. Phys.* **155**, 92 (2015)
4. A. Singh, S. Suri, P. Kumar, B. Kaur, A.K. Thakur, V. Singh, *J. Alloys Compd.* **764**, 599 (2018)
5. V. Trukhanov, V.O. Turchenko, I.A. Bobrikov, S.V. Trukhanov, I.S. Kazakevich, A.M. Balagurov, *J. Magn. Magn. Mater.* **393**, 253 (2015)
6. V. Turchenko, V.G. Kostishyn, S. Trukhanov, F. Damay, F. Porcher, M. Balasoiu, N. Lupu, B. Bozzo, I. Fina, A. Trukhanov, J. Waliszewski, K. Recko, S. Polosan, *J. Alloys Compd.* **821**, 153412 (2020)
7. S. Dagar, A. Hooda, S. Khasa, M. Malik, *J. Alloys Compd.* **826**, 154214 (2020)
8. S.V. Trukhanov, A.V. Trukhanov, V.A. Turchenko, A.V. Trukhanov, E.L. Trukhanova, D.I. Tishkevich, V.M. Ivanov, T.I. Zubar, M. Salem, V.G. Kostishyn, L.V. Panina, D.A. Vinnik, S.A. Gudkova, *Ceram. Int.* **44**, 290 (2018)
9. V. Turchenko, A. Trukhanov, S. Trukhanov, M. Balasoiu, N. Lupu, *J. Magn. Magn. Mater.* **477**, 9 (2019)
10. O.S. Yakovenko, L.Y. Matzui, L.L. Vovchenko, A.V. Trukhanov, I.S. Kazakevich, S.V. Trukhanov, Y.I. Prylutskyy, U. Ritter, *J. Mater. Sci.* **52**, 5345 (2017)
11. M.M. Salem, L.V. Panina, E.L. Trukhanova, M.A. Darwish, A.T. Morchenko, T.I. Zubar, S.V. Trukhanov, A.V. Trukhanov, *Compos. B* **174**, 107054 (2019)
12. R.S. Devan, C.M. Kanamadi, S.A. Lokare, B.K. Chougule, *Smart Mater. Struct.* **15**, 1877 (2006)
13. R.S. Devan, B.K. Chougule, *Phys. B* **393**, 161 (2007)
14. S. Dagar, A. Hooda, S. Khasa, M. Malik, *J. Alloys Compd.* **806**, 737 (2019)
15. M.A. Almessiere, A.V. Trukhanov, Y. Slimani, K.Y. You, S.V. Trukhanov, E.L. Trukhanova, F. Esa, A. Sadaqati, K. Chaudhary, M. Zdorovets, A. Baykal, *Nanomaterials*. **9**, 202 (2019)
16. M.V. Zdorovets, A. Arbuz, A.L. Kozlovskiy, *Ceram. Int.* **46**, 6217 (2020)
17. Z.V. Mocanu, G. Apachitei, L. Padurariu, F. Tudorache, L.P. Curecheriu, Z.V. Mocanu, G. Apachitei, L. Padurariu, F. Tudorache, L.P. Curecheriu, HAL Id : hal-00736283 (2012)
18. Ashima, S. Sanghi, A. Agarwal, Reetu, N. Ahlawat, Monica, *J. Appl. Phys.* **112**, 014110 (2012)
19. D.R. Patil, S.A. Lokare, S.S. Chougule, B.K. Chougule, *Phys. B* **400**, 77 (2007)

20. K.W. Wagner, *Ann. Phys.* **345**, 817 (1913)
21. C.G. Koops, *Phys. Rev.* **83**, 121 (1951)
22. J. William, D. Callister, D.G. Rethwisch, *Mater. Sci. Eng.* **536** (2013)
23. C.M. Kanamadi, S.R. Kulkarni, K.K. Patankar, S.S. Chougule, S.J. Patil, B.K. Chougule, *J. Mater. Sci.* **42**, 5080 (2007)
24. S.S. Chougule, D.R. Patil, B.K. Chougule, *J. Alloys Compd.* **452**, 205 (2008)
25. H.F. Zhang, S.W. Or, H.L.W. Chan, *J. Alloys Compd.* **509**, 6311 (2011)
26. M.V. Zdorovets, A.L. Kozlovskiy, *Vacuum* **168**, 108838 (2019)
27. M. Rawat, K.L. Yadav, *Smart Mater. Struct.* **24**, 45041 (2015)
28. F.S. Moghadasi, V. Daadmehr, M. Kashfi, *J. Magn. Magn. Mater.* **416**, 103 (2016)
29. B.K. Barick, K.K. Mishra, A.K. Arora, R.N.P. Choudhary, D.K. Pradhan, *J. Phys. D* **44**, 355402 (2011)
30. S. Thakur, R. Rai, I. Bdikin, M.A. Valente, H. Pradesh, C.U. De Santiago, *I. Introduction*, **19**, 1 (2016)
31. R. Kumari, N. Ahlawat, A. Agarwal, S. Sanghi, M. Sindhu, N. Ahlawat, *J. Alloys Compd.* **676**, 452 (2016)
32. R.N. Bhowmik, M.C. Aswathi, *Compos. B* **160**, 457 (2019)
33. J. Ondru, Š. Csáki, V. Trnovcová, Š. Igor, *Appl. Clay Sci.* **154**, 36 (2018)
34. R. Dahiya, A. Agarwal, S. Sanghi, Ashima, N. Ahlawat, *J. Phys. D* **45**, 165001 (2012)
35. V. Trukhanov, L.S. Lobanovski, M.V. Bushinsky, I.O. Troyanchuk, H. Szymczak, *J. Phys.* **15**, 1783 (2003)
36. M.V. Zdorovets, A.L. Kozlovskiy, Study of the stability of the structural properties of CeO₂ microparticles to helium irradiation. *Surf. Coat. Technol.* **383**, 125286 (2020)
37. S.V. Trukhanov, I.O. Troyanchuk, A.V. Trukhanov, I.M. Fita, A.N. Vasil'ev, A. Maignan, H. Szymczak, *JETP Lett.* **83**, 33 (2006)
38. I. Kozlovskiy, M. Kenzhina, Zdorovets. *Ceram. Int.* **45**, 8669 (2019)
39. Z. Gao, Y. Pu, M. Yao, Q. Jin, Y. Wang, H. Zheng, *Ceram. Int.* **43**, 85 (2017)
40. F. Garbayo, A. Baiutti, A.T. Morata, *J. Eur. Ceram. Soc.* **39**, 101 (2019)
41. S.V. Trukhanov, A.V. Trukhanov, C.E. Botez, A.H. Adair, H. Szymczak, R. Szymczak, *J. Phys. Condens. Matter.* **19**, 266214 (2007)

Publisher's Note Springer Nature remains neutral with regard to jurisdictional claims in published maps and institutional affiliations.